Acoustic pulse propagation in a fluctuating ocean with range-dependent sound-speed profile

W. R. Chang and J. H. Tarng
Department of Communication Engineering, Chiao-Tung University, Hsin-Chu, Taiwan, Republic of China

(Received 13 January 1995; accepted for publication 20 November 1995)

When an acoustic pulse propagates in a randomly fluctuating ocean with a deterministic sound-speed profile, it is distorted since every frequency component experiences different extents of scattering from the random inhomogeneity and echo numbers. Here, the split-step method is used to simulate an acoustic pulse with a 3-kHz carrier propagating through a turbulent ocean with range-independent/-dependent sound-speed profiles. It is found that (1) the ocean is a frequency-selective fading channel; (2) the received pulse profile is dependent on the received depth, sound-speed distribution, fluctuation strength, and scale length of turbulence in oceans; (3) the rms pulsewidth is broadened by several times its initial value as a consequence of pulse echoes and pulse wandering of every pulse realization of the ensemble; (4) the rms pulsewidth is increased when the fluctuation strength increases or the scale length decreases; and (5) the statistical properties of the propagating pulse are similar for both the range-independent and -dependent cases in the mean square sense.

PACS numbers: 43.30.Bp, 43.30.Cq

INTRODUCTION

Recently, acoustic pulse propagation in the ocean has attracted much attention because of its practical importance.[1–3] The pulse is distorted due to the existence of the sound-speed profile and turbulence. Multiple-path propagation of acoustic waves can occur in the ocean because of the vertical sound-speed profile. In addition, the sound speed has random temporal and spatial variations due to internal waves and the fine structure of temperature in the ocean.[4,5] Because of these stochastic fluctuations, each frequency component of the pulse will be scattered to a different extent. Distortion and broadening of the pulse after propagation is expected.

The broadening and distortion of a pulse when it is propagating through a random medium has been studied both theoretically and experimentally.[3,6,7] The stochastic properties of the pulsewidth provides the information about the broadening. Physically, there exist two possible causes for this broadening. It may be due to the fact that the pulse is spread in time as a consequence of scattering from each realization of the ensemble. It may also come about because of the wandering of the pulse, that is, the arrival time of the pulse differs from one member of the acoustic ensemble to another. However, when there exists a deterministic inhomogeneity, there are pulse echoes due to multipath propagation and this may be coupled with the random fluctuation of the inhomogeneity to change both the arrival time of echo and number of the echoes. Hence, the acoustic pulse propagation in a turbulent ocean is affected both by the deterministic sound-speed profile and random fluctuation of sound-speed profile. Exploration of the coupling effect between turbulence and sound-speed profile on acoustic propagation becomes an interesting and important issue.

Basically, the evaluation of the average intensity of the pulse depends on that of the two-frequency mutual coherence function.[8] However, it is usually difficult to compute this coherence function. The temporal moment method[9] was introduced to avoid this difficulty. In this method, the temporal moments can be evaluated without an explicit expression for the two-frequency mutual coherence function.[9] These temporal moments represent important statistical parameters of the randomly distorted pulse. However, the temporal moment method can only deal with the case of range-independent sound-speed profile and with the propagation range to be sufficiently short that the ray trajectory does not pass the propagation axis.[10] With such limitations, efforts will resort to the numerical methods.

Calculation of the propagation of acoustic energy in a realistic ocean where velocity is a function of both range and depth is of continuous interest.[11] Recent developments in the analysis of weakly range-dependent guiding channels, using the spectral approach, have led to the development of a global spectral Green's function for range-dependent waveguides. Kamel and Felsen[12] generalized the method of characteristic Green's function for a two-dimensional ocean waveguide to accommodate weak range dependence. Lu and Felsen[13] developed approximate adiabatic transforms that accomplish for weakly range-dependent oceanic waveguides what the rigorous transform does exactly for the range-independent case. However, both approaches only deal with the deterministic cases, research in WPRM (wave propagation in random media) has scarcely been reported. An alternate way is to use the numerical approach.

Many numerical methods have been proposed for the solutions of wave propagation problems. Among these are the Fourier split-step,[14] implicit finite difference (Crank–Nicholson),[15] and method of lines based on the Adam–Bashforth formula.[16] Here, the split-step method is used to calculate the temporal behavior of stochastic waves. It is unconditionally stable and computationally efficient. The algorithm does, however, require periodic boundary conditions in z because of its use of the finite Fourier transform.

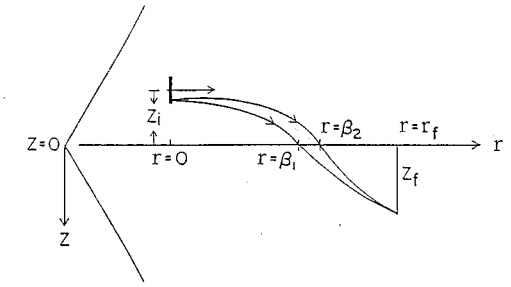

FIG. 1. Geometry of acoustic pulse propagation in the ocean. The bilinear sound-speed profile with minimum sound speed at the depth $z=0$ is shown. The point source approximated by a Gaussian beam with the center at the depth z_i is launched horizontally in the plane $r=0$. Multipath propagation happens in this situation. The receiving point located at the range r_f and depth z_f.

This requirement is handled by introducing an artificial horizontal bottom boundary below the physical bottom, and assuming that the field satisfies a zero boundary condition there.

In our research, an acoustic pulse propagates through a turbulent deep ocean with range-dependent sound-speed profile is explored. This means that the deterministic profile is dependent on both the ocean depth and range distance. The geometry of the problem is illustrated in Fig. 1. A point source and a point receiver are placed at $z=z_i$ and $z=z_f$, respectively. The split-step method is employed to simulate the propagation of a cw acoustic wave and temporal moments are computed to estimate the average arrival time and width spreading of an acoustic pulse. According to the spatial autocorrelation function of the turbulence, we generate the multiple phase-screen (MPS) to represent both the contributions of the deterministic and random inhomogeneities.[17] Results show that the effects of random scattering on the arrival time are negligibly small. However, random scattering will significantly broaden the pulse especially when the range is long. Dependence of the arrival time and pulse width on the variance and scale size of turbulence are also given.

The rest of this paper is organized as follows, in Sec. I the time-harmonic wave equation and the pulse propagation are formulated. The split-step method and generation of phase screen are introduced in Sec. II. In Sec. III numerical examples and discussion are demonstrated. Finally, the results are summarized and a conclusion is drawn.

I. WAVE EQUATION AND FORMULATION

In an ocean cylindrically symmetric about an axis containing a point time-harmonic source, the acoustic pressure $p(r,z)$ satisfied the reduced wave or Helmholtz equation

$$r^{-1}(rp_r)_r+p_{zz}+k_0^2n^2(r,z)p=0, \tag{1}$$

where $k_0=2\pi f/c_0$, f is the frequency of the source, and the index of refraction, $n(r,z)$, is given by $n(r,z)=c_0/c(r,z)$, where the constant c_0 is a reference sound speed, and $c(r,z)$ is the sound speed at the point (r,z).

In the parabolic equation method for solving the reduced wave equation, the solution $p(r,z)$ is written in the form

$$p(r,z)=\psi(r,z)H_0^{(1)}(k_0r), \tag{2}$$

reasoning that the primary radial dependence of the field in terms of an outward propagating radial wave is represented by the Hankel function $H_0^{(1)}(kr)$. If the receiver is assumed to be many wavelengths away from the source $(k_0r\gg1)$, and with the paraxial approximation assumption, $|\psi_{rr}|\ll|2ik_0\psi_r|$, then the Leontovich–Fock[18] parabolic equation

$$2ik_0\psi_r+\psi_{zz}+k_0^2[n^2(r,z)-1]\psi=0 \tag{3}$$

for the transmitted field is obtained from Eq. (1). The approximation was first introduced in underwater acoustics by Tappert and Hardin.[19] The application of the parabolic approximation in ocean acoustics rests on two requirements: (1) that local variations of the acoustic refractive index are small, and (2) that effective propagation paths are limited to a narrow aperture centered about the forward scattered direction.[20]

In a turbulent ocean, the sound speed can be expressed as

$$c(r,z)=c_0[1+U(z)+\mu(r,z)], \tag{4}$$

where $U(z)$ is a dimensionless function of the depth z representing the deterministic sound-speed profile, and μ is a random, zero-mean function of position representing the relative fluctuation caused by medium fluctuations such as the internal wave. The wave equation for an acoustic wave is unaffected by the time dependence of μ because μ has only components with very low frequency. Substituting Eq. (4) in Eq. (3) and neglecting ψ_{rr} and the second and higher-order terms of U and μ, the standard parabolic equation is derived and given by

$$2ik_0\psi_r+\psi_{zz}-2k_0^2(U+\mu)\psi=0. \tag{5}$$

For pulse propagation, the distortions of a pulse in a random medium are attributed to the different scattering character of the frequency components of the pulse. The pulse after propagation can be formulated by the equation

$$p(r,t)=\int_{-\infty}^{\infty}F(\omega)\psi(r,\omega)\exp\{-i[\omega t-k(\omega)r]\}d\omega + \text{c.c.} \tag{6}$$

Here, the pulse $p(r,t)$ propagating along the r direction, which is designated as the propagation axis, has been Fourier decomposed. The notation $F(\omega)$, as a function of the angular frequency ω, stands for the spectrum of the pulse; $k(\omega)$ is the wave number along the propagation axis; and the complex amplitude $\psi(r,\omega)$ describes the effects of random scattering of a single frequency wave with the initial condition $\psi(0,\omega)=1$. Here, we assume an initial Gaussian pulse which is given by

$$p(0,t)=\exp(-t^2/T_0^2)\cos(\omega_c t), \tag{7}$$

where (ω_c) is the carrier frequency and $T_0/\sqrt{2}$ is the pulsewidth. After a Fourier transform, the frequency spectrum is given by

$$F(\omega)=(T_0\sqrt{\pi}/2)\{\exp[-T_0^2(\omega-\omega_c)^2/4] + \exp[-T_0^2(\omega+\omega_c)^2/4]\}. \quad (8)$$

From Eq. (5), we can calculate $\psi(r,\omega)$ for propagation of each frequency component by using the split-step method. By substituting $\psi(r,\omega)$ and $f(\omega)$ into Eq. (6), the real pulse shape $p(r,t)$ is computed.

II. SPLIT-STEP METHOD

A. Split-step method

To solve Eq. (5), the split-step method is proposed. This method is of exponential accuracy in z and second-order accuracy in r.[14,21] A phase screen is inserted to represent the phase change due to the existence of random and deterministic inhomogeneities, in an infinitesimal increment Δ_r in range. This effect has been separated with the diffraction effect. Hence, the evolution of complex amplitude in a range Δ_r is given by

$$\psi(r+\Delta_r,z)=e^{i\Delta_r[A-k_0(U+\mu)]}\psi(r,z), \quad (9)$$

where $A=(1/2k_0)\partial_{zz}$ is an operator representing the diffraction effect. By using the Fourier transformation,

$$\psi(r+\Delta_r,z)=F^{-1}[e^{-ik_z^2\Delta_r/(2k_0)}F[e^{-ik_0(U+\mu)\Delta_r}\psi(r,z)]], \quad (10)$$

where $F\{\cdot\}$ denotes the Fourier transformation from z space to k_z space, $F^{-1}\{\cdot\}$ denotes the inverse Fourier transformation.

Notice that when the spatial parameter z does the discrete Fourier transformation (DFT) to the spatial frequency k_z, the sampling interval Δ_z is chosen to avoid aliasing in spatial frequency, i.e., $(\Delta_z)^{-1}\geqslant 2(k_z)_{\max}$, where $(k_z)_{\max}$ represents the maximum spatial frequency of the field distribution on the transverse axis z. Here, $\Delta_z=1/2(k_z)_{\max}$, and the spatial frequency interval Δ_{k_z} is equal to $2\pi/N\Delta_z$, where N is the total number of spatial sampling points, i.e., $N-1$ spatial intervals are considered. The procedures are repeated for all screens until the observing plane is reached. It has been observed that this method is the discrete version of the path integral method of wave scattering analysis for infinitesimal range Δ_r and, therefore, is an exact solution to the parabolic equation under the restrictions imposed by the finite screen size and sampling interval.

To specify the statistics of each phase screen, the calculation of the correlation function and spatial spectrum of phase variations are needed. In the simulation, the fluctuation in each slab is assumed not to change the amplitude of the field ψ. However, the phase fluctuation causes the amplitude to fluctuate during propagation through many Δ_r, because of the diffraction effect.

Ignoring the diffraction and deterministic refraction effects, the phase correlation function is defined by

$$B_\theta(z_1-z_2)=k_0^2\int_0^{\Delta_r}\int_0^{\Delta_r}\langle\mu(r,z_1)\mu(r',z_2)\rangle dr\ dr' = k_0^2\Delta_r A_\mu(z_1-z_2), \quad (11)$$

where B_θ is the correlation function of accumulated phases at depths z_1 and z_2. In simplifying Eq. (11), it is assumed that $\Delta_r>l_r$ where l_r is the scale length of the irregularities in r direction. The function A_μ is the integrated correlation function of the sound-speed fluctuations and may be expressed in terms of the spatial spectrum of irregularities $\Phi_\mu(k_z)$ as

$$A_\mu(z)=2\pi\int_{-\infty}^{\infty}\Phi_\mu(k_z)e^{ik_z z}\,dk_z. \quad (12)$$

Therefore, the relationship between the phase spectrum of each screen and refractive index spectrum is

$$\Phi_\theta(k_z)=2\pi k_0^2\Delta_r\Phi_\mu(k_z). \quad (13)$$

B. Phase-screen generation

The goal here is to generate a discretized and stationary random function $\theta(n\Delta z)$ which represents the phase of nth grid point of each phase screen in the transversal direction with sampling spacing Δz of two neighboring points. In continuous notation, the phase may be written as the Fourier transformation by

$$\theta(z)=\int_{-\infty}^{\infty}K_\theta(k_z)e^{ik_z z}\,dk_z. \quad (14)$$

In the discrete case, Eq. (14) becomes

$$\theta(n\Delta z)=\sum_{m=0}^{N-1}K_\theta(m\Delta k_z)e^{i(2\pi/N)mn}\,\Delta k_z, \quad (15)$$

where $n=0,...,N-1$. It can be shown[21] that

$$K_\theta(m\Delta k_z)=r_m[\Phi_\theta(m\Delta k_z)]^{1/2}[L/2\pi]^{1/2}, \quad (16)$$

where $\Phi_\theta(m\Delta k_z)$ represents discrete values of the known desired phase spectral density and L is the vertical length of the phase screen grid. The complex number r_m is given as the sum of two independent Gaussian random variables with zero mean and variances of unity, i.e., $r_m=A_m+iB_m$. The values of A_m and B_m can be generated numerically by sampling from a pseudorandom sequence of numbers with a Gaussian distribution.[22] Since the phase of an individual phase screen is real, we may choose either the real or imaginary part of $\theta(n\Delta z)$ from Eq. (15). Since the real and imaginary parts are independent, they are used to represent the random phases of two independent screens, respectively.

III. NUMERICAL EXAMPLES AND DISCUSSIONS

Here, numerical examples of acoustic pulse propagation in turbulent oceans considering range-independent or range-dependent sound-speed profile are illustrated. In our computation, a bilinear sound-speed profile is assumed and $U(z)$ is given by $U(z)=b_1z$, $z<0$, and $U(z)=b_2z$, $z\geqslant 0$. Meanwhile, the following parameters are chosen: $z_i=-75$ m, $b_1=-b_2=-1.1\times10^{-5}(\mathrm{m}^{-5})$, $C_0=1500$(m/s), the propagation distance $x_f=10$ (km), $T_0=1.5$ ms and the carrier frequency of the pulse signal 3 kHz. In subsections A and B a Gaussian correlation function of $\langle\mu\rangle$ is assumed, i.e., $B_\mu(r,z)=\langle\mu^2\rangle\exp(-(r^2+z^2)/l^2)$, where $\langle\mu^2\rangle$ and l are the mean square fluctuation and scale length of μ. In subsection

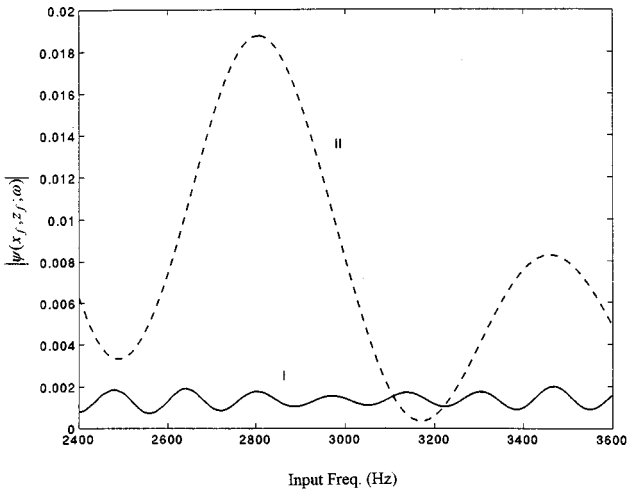

FIG. 2. The curves of received amplitude as a function of input frequency I and II are shown for $z_f=-25$ m and $z_f=50$ m with $\langle\mu^2\rangle=0$.

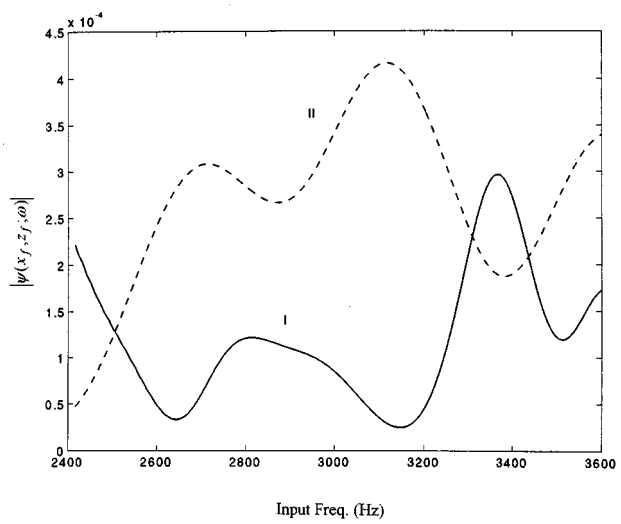

FIG. 3. The curves of received amplitude as a function of input frequency I and II are shown for $\langle\mu^2\rangle=10^{-6}$ and $\langle\mu^2\rangle=10^{-7}$, respectively, for $l=74$ m and $z_f=50$ m.

C, both the temperature fine structure and the power law spectra are considered for the case of range independence.

In the creation of the random phase screen, the complex random number A_m+iB_m is simulated by calling the subroutine *drnnoa* in IMSL (International Mathematical Statistic Library). Here, $N=4096$, 100 slabs are assumed in employing the split-step method, i.e., $\Delta_r=100$(m) and $\Delta_z\approx 0.76$(m). The notations Δ_r and Δ_z represent the space sampling distance in the range and depth directions, respectively. To avoid the effect of spatial aliasing, a spatial Gaussian distribution along the z direction is used to replace the point source, i.e., $\psi(0,z)=(i\pi^{1/2}/\omega)\exp[-(z-z_0)^2/\omega^2]$. The initial beamwidth ω is chosen to equal $4/\pi$ to avoid the spatial sampling aliasing and to be sure that the span of the spatial frequency in k_z domain is wide enough to keep necessary information during the inverse descrete Fourier transformation.

Here, 60, 80, 120, 140, 160, and 200 trial runs are individually executed for several cases and the statistical first and second moments of the propagating pulse are evaluated for each trial run. By comparing the moments of each trial run, it is found that 80 trial runs already give a stable result. Therefore, 80 trial runs are chosen to simulate the pulse propagating through the fluctuating ocean and the average pulse profile and rms (root mean square) of the received pulse are evaluated by the 80 realizations.

A. Range-independent sound-speed profile

In Fig. 2, the received amplitude as a function of input frequency is illustrated by curve I and II at receiving depths -25 and 50 m, respectively, where $\langle\mu^2\rangle=0$, i.e., the sound-speed profile is deterministic. It shows that the ocean is a frequency-selective fading and the fading depth varies with the ocean depth. It is obvious that the fading is caused by the multipath interference. The fading oscillates faster but weaker at $z_f=-25$ m than that at $z_f=50$ m. It is because that at the depth -25 m weak but numerous micromultiple paths arrive, therefore, to yield a fast but shallow-depth fading. On the other hand, only strong but few macromultiple paths arrive at the depth $z_f=50$ m, which give slower but deeper fading. In the case of random fluctuation of sound-speed profile, the received amplitude of frequency response averaging over 80 realizations is shown in Fig. 3 with curves I and II for $\langle\mu^2\rangle=10^{-6}$ and 10^{-7}, respectively. Here, $l=74$ m. By comparing the both curves with the curve II in Fig. 2, it shows that the random fluctuating of the ocean can increase the number of the micromultiple paths, hence, it leads to a faster fading when the fluctuating strength is increased. By giving the initial spectral density function of the pulse, i.e., Eq. (8) is used, the received pulse can be calculated. In the case with no turbulence the received pulse profile is shown in Fig. 4 and at depth $z_f=-25$, 50, and 75 m, respectively. Owing to the multipath propagation, echoes are received. Number of the received echo is changed with the depth.

When there is random fluctuations, two individual realizations of pulse delay profile are illustrated separately by

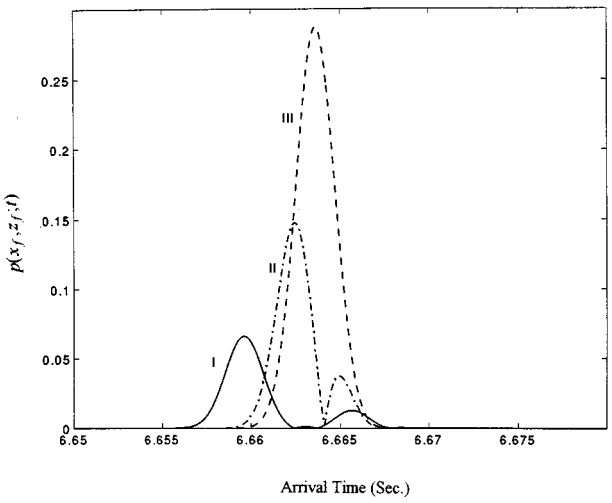

FIG. 4. The received pulse profiles I, II, and III are shown for $z_f=-25$, 50, and 75 m with $\langle\mu^2\rangle=0$.

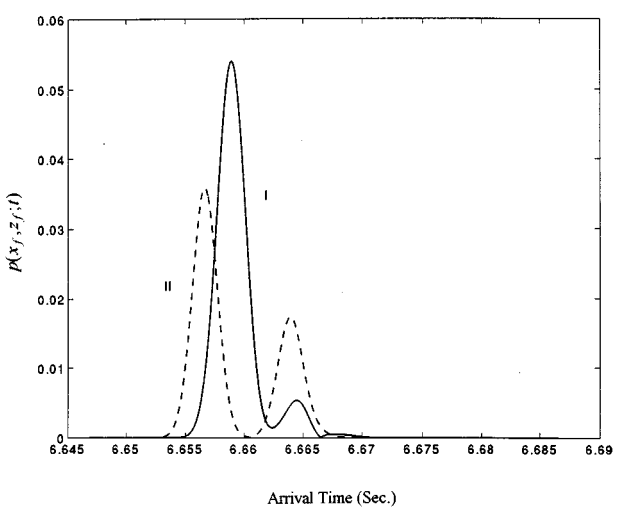

FIG. 5. Two realizations of the received pulse profile for $z_f=50$ m, $\langle\mu^2\rangle=10^{-6}$, $l=74$ m.

curves I and II in Fig. 5 for $\langle\mu^2\rangle=10^{-6}$, $l=74$, and $z_f=50$ m. By comparing these two figures, it reveals that the pulse is wandering and the magnitude and number of echoes are varied which leads to the pulse broadening. However, the pulse itself is spread only slightly in time. After averaging over 80 realizations, the average pulse profiles I, II, III, and IV are shown in Fig. 6 for $\langle\mu^2\rangle=10^{-6}$, 10^{-7}, 10^{-8}, and 10^{-15}, respectively, where $z_f=50$ m and $l=74$ m. By comparing the curve IV in Fig. 6 with the curve II in Fig. 4, it shows that when $\langle\mu^2\rangle=10^{-15}$ the average pulse profile is approaching that of the limiting case $\langle\mu^2\rangle=0$. The root mean square pulsewidth of the first three profiles is calculated from the 80 realizations and given by 1.69, 1.46, and 1.41 ms, in the corresponding order. It shows that the larger fluctuation of sound-speed distribution gives larger broadening of the receiving pulsewidth. The rms pulsewidth after propagation increases from 1.33 to 1.59 times of the initial rms pulsewidth which is equal to 1.06 ms. The broadening is a consequence of echo arrivals, due to multipath propagation, and

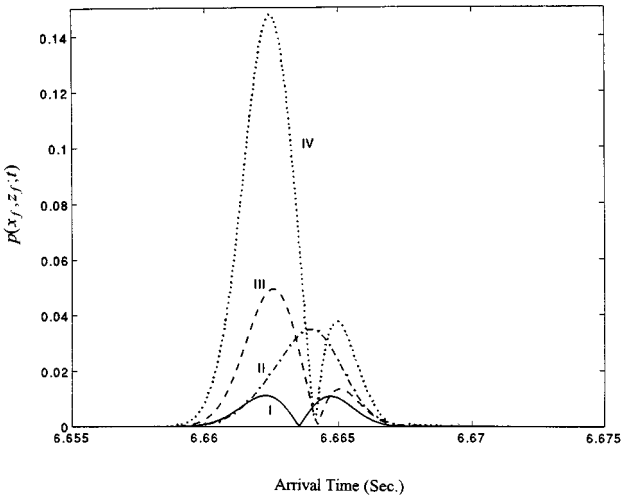

FIG. 6. The average pulse profiles I, II, III, and IV are shown for $\langle\mu^2\rangle=10^{-6}$, 10^{-7}, 10^{-8}, and 10^{-15}, respectively, for $l=74$ m, and $z_f=50$ m.

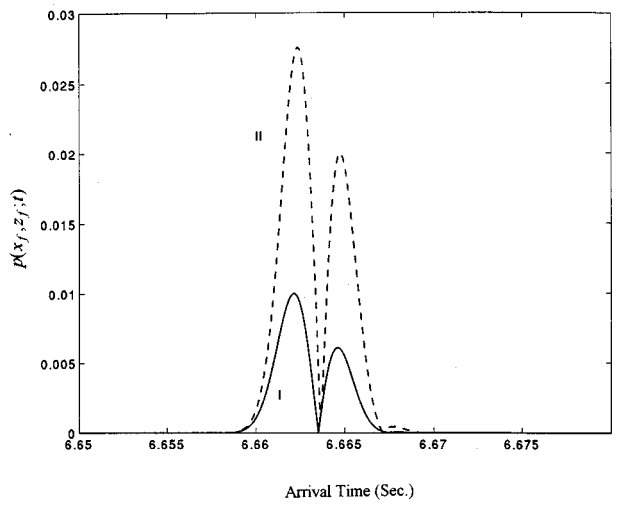

FIG. 7. The average pulse profiles I and II are shown for $l=40$ m and $l=10$ m, respectively, for $\langle\mu^2\rangle=10^{-7}$.

pulse wandering of every pulse realization of the ensemble, due to scattering form random inhomogeneity. In Fig. 7, the average pulse profile is shown by curves I and II for the scale length $l=40$ and 10 m, respectively, where $\langle\mu^2\rangle=10^{-7}$, $z_f=50$ m. After calculation, the rms pulsewidth equals 1.68 and 1.80 ms for $l=40$ and 10 m, respectively. It shows that when l decreases, the rms pulsewidth increases. It is because that a decrease in the scale length leads to an increase in the decorrelation among multiple paths, thus, the rms of pulsewidth increases. It is found that the change of mean arrival time of the sampled pulses is very small when the receiving depth, $\langle\mu^2\rangle$ or l is changed. It is consistent with the result in Ref. 10.

B. Range-dependent sound-speed profile

In this case, the sound channel axis is assumed to increase in depth by 50 m uniformly over 10-km range distance, hence, the parabolic approximation is still applicable. The received pulse profile at depths -25, 50, and 75 m is illustrated as curves I, II, and III, respectively, in Fig. 8. The pulse delay profile as well as the acoustic energy distribution along the depth are different from those in the range independent. Most of the received acoustic energy is concentrated above the channel axis because of the downtilted axis. In Fig. 9, the average pulse profile is shown for $\langle\mu^2\rangle=10^{-6}$ and 10^{-7}, by curves I and II, respectively. Here, the received depth $z_f=50$ m and $l=74$ m. The increase of fluctuation strength can change the arrival times and shapes of echoes, thus rms pulsewidth is increased as well.

C. Temperature fine structure and power-law spectra

To be more realistic, the sound-speed fluctuation due to the temperature fine structure is considered and its correlation function of μ, i.e., $B_\mu(r,z)$, is given by $\langle\mu^2\rangle\exp(-|z|/z_0)\exp(-r^2/l^2)$ with typical value of $z_0=2$ m and $l=74$ m.[5] Its numerical example of average pulse profile is illustrated in Fig. 10 at depths -25, 50, and 75 m for curves I, II, and III, respectively. Here, $\langle\mu^2\rangle=10^{-9}$. The re-

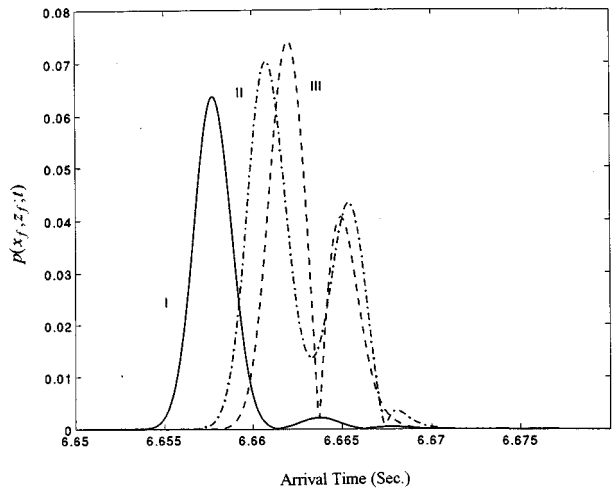

FIG. 8. The received pulse profiles I, II, and III are shown for $z_f=-25$, 50, and 75 m with $\langle\mu^2\rangle=0$.

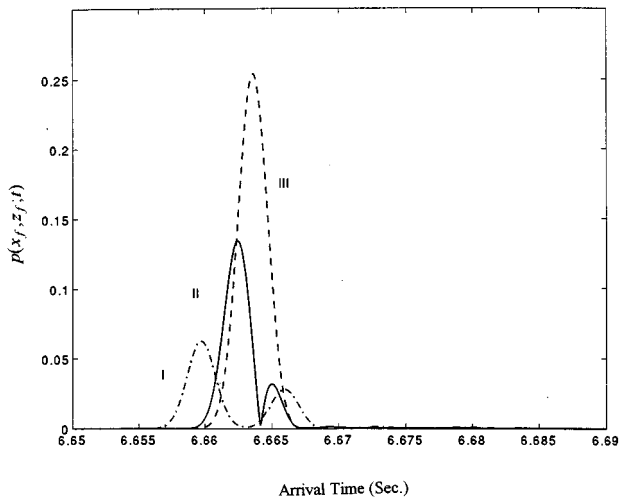

FIG. 10. The average pulse profiles I, II, and III are drawn at depths $z_f=-25$, 50, and 75 m, respectively, for the case of temperature fine structure with $\langle\mu^2\rangle=10^{-9}$, $z_0=2$ m and $l=74$ m.

spective rms pulsewidths are 6.2, 4.1, and 2.9 ms. The temperature fine structure causes larger pulse broadening which is due to the small scale length in the vertical direction. In Fig. 11, the average pulse profiles I and II are drawn for the case of the power law spectrum with $C_n^2=10^{-7}$ and $C_n^2=10^{-9}$, respectively, for $z_f=50$ m. The respective rms pulsewidth are 3.7 and 1.8 ms. A larger fluctuation strength yields a larger rms pulsewidth. Here, the Kolmogorov spectrum is used as an example and its spectrum is given by $\Phi_\mu(k_z)=0.033C_n^2k_z^{-11.3}$.

IV. CONCLUSION

In this research, the statistical properties of an acoustic pulse after propagating through a turbulent ocean with range-independent/dependent sound-speed profiles are investigated. The split-step method is used to evaluate the propagating effect on every frequency component of the pulse. The layer structure of the ocean forms the macrostationary paths scattered by the random inhomogeneity and turns into many microstationary paths. Hence, the interferences among these macrostationary paths are smoothed. It is found that (1) the ocean is a frequency-selective fading channel because of the multipath propagation and turbulence scattering; (2) the received pulse profile is dependent on the received depth, deterministic sound-speed distribution, fluctuation strength, and scale length of turbulence in oceans; (3) the rms pulsewidth can be broadened several times the initial pulsewidth; (4) the increase in fluctuation strength or decrease in the scale length increases the rms pulsewidth; and (5) the statistical properties of the pulse are similar for both the range-independent and dependent sound-speed profiles but the acoustic energy distributions are different from each other owing to the varying of sound-channel axis. To predict acoustic pulse propagation in an ocean, a complicated propagation environment, numerical approaches are necessary. The split-step method can handle the problems that satisfy the forward scattering

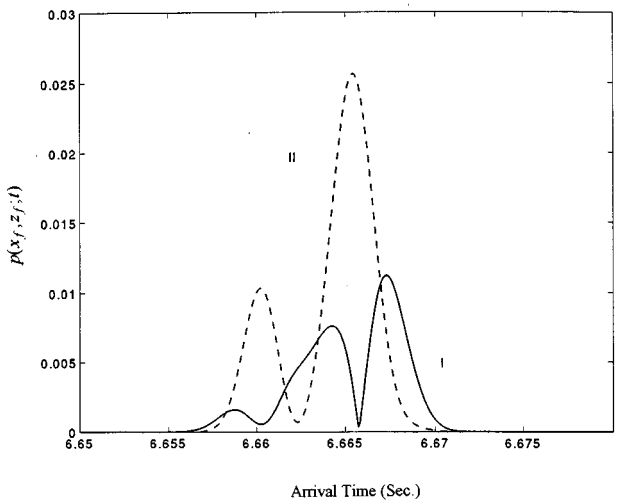

FIG. 9. The average pulse profiles I and II are shown for $\langle\mu^2\rangle=10^{-6}$ and $\langle\mu^2\rangle=10^{-7}$, respectively, for $l=74$ m, and $z_f=50$ m.

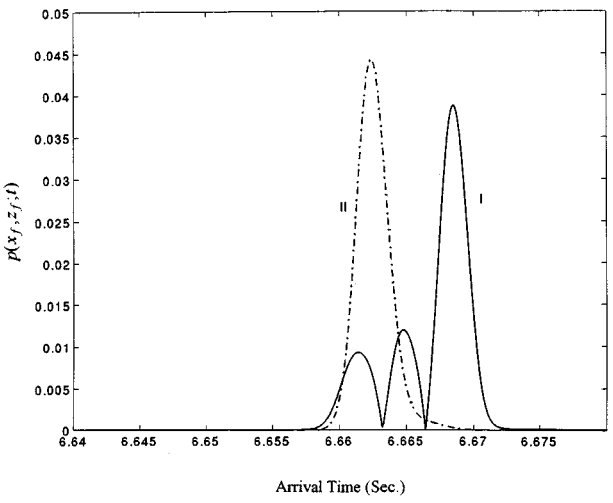

FIG. 11. The average pulse profiles I and II are drawn for the case of power law spectrum with $C_n^2=10^{-7}$ and $C_n^2=10^{-9}$, respectively, for $z_f=50$ m.

approximation very efficiently. In the near future, a broadband signal and a 3-D geometry problem will be explored.

ACKNOWLEDGMENT

This research was supported by National Science Council of Taiwan under the Project No. NSC82-0209-E009-404.

[1] W. E. Kohler, ''Pulse propagation in a randomly perturbed ocean: single pulse statistics,'' J. Acoust. Soc. Am. **68**, 1177–1183 (1980).
[2] R. Kashen, S. M. Flatte, and S. A. Reynolds, ''Path-integral treatment of acoustic mutual coherence functions for rays in a sound channel,'' J. Acoust. Soc. Am. **77**, 1716–1722 (1985).
[3] J. A. Colosi, S. M. Flatte, and C. Bracher. ''Internal-wave effects on 1000-km oceanic acoustic pulse propagation: Simulation and comparison with experiment,'' J. Acoust. Soc. Am. **96**, 452–468 (1994).
[4] R. Esswein and S. Flatte, ''Calculation of the phase structure function density from oceanic internal waves,'' J. Acoust. Soc. Am. **70**, 1387–1396 (1981).
[5] S. Unni and C. Kaufman, ''Acoustic fluctuations due to the temperature fine structure of the ocean,'' J. Acoust. Soc. Am. **69**, 676–680 (1981).
[6] E. A. Bucher, ''Computer simulation of light pulse propagation for communication through clouds,'' Appl. Opt. **12**, 2391–2400 (1973).
[7] C. H. Liu and K. C. Yeh, ''Propagation of pulsed beamwaves through turbulence cloud, rain or fog,'' J. Opt. Soc. Am. **67**, 1216–1266 (1977).
[8] R. L. Fante, ''Two-position, two-frequency mutual-coherence function in turbulence,'' J. Opt. Soc. Am. **71**, 1446–1451 (1981).
[9] K. C. Yeh and C. H. Liu, ''An investigation of temporal moments of stochastic waves,'' Radio Sci. **12**, 671–680 (1977).
[10] J. H. Tarng, L. K. Wang, C. C. Yang, and S. T. McDaniel, ''Arrival time and pulse width of acoustic pulses in a turbulent ocean,'' J. Acoust. Soc. Am. **84**, 1802–1807 (1988).
[11] L. E. Estes and G. Fain, ''Numerical technique for computing the wide-angle acoustic field in an ocean with range-dependent velocity profiles,'' J. Acoust. Soc. Am. **62**, 38–43 (1977).
[12] A. Kamel and L. B. Felsen, ''Spectral theory of sound propagation in an ocean channel with weakly sloping bottom,'' J. Acoust. Soc. Am. **73**, 1120–1130 (1983).
[13] I. T. Lu and L. B. Felsen, ''Adiabatic transforms for spectral analysis and synthesis of weakly range-dependent shallow ocean Green's functions,'' J. Acoust. Soc. Am. **81**, 897–911 (1987).
[14] R. H. Hardin and F. D. Tappert, ''Application of the split-step Fourier method to the numerical solution of nonlinear and variable coefficient wave equation,'' SIAM Rev. **15**, 423 (1973).
[15] D. Lee, G. Botseas, and J. S. Papadakis, ''Finite-difference solution to the parabolic wave equation,'' J. Acoust. Soc. Am. **70**, 795 (1981).
[16] D. Lee and J. S. Papadakis, ''Numerical solutions of underwater acoustic wave propagation problems,'' Tech. Rep. 5929, Naval Underwater System Center, New London, CT, February 1984.
[17] D. L. Knepp, ''Multiple phase-screen calculation of the temporal behavior of stochastic waves,'' Proc. IEEE **71**(6), 722–737 (1983).
[18] F. D. Tappert and D. Lee, ''A range refraction parabolic equation,'' J. Acoust. Soc. Am. **76**, 1797–1803 (1984).
[19] F. D. Tappert, ''The parabolic equation method,'' in *Lecture Notes in Physics*, edited by J. B. Keller and J. S. Papadakis (Springer-Verlag, New York, 1977), No. 70.
[20] F. B. Jensen, W. A. Kuperman, M. B. Porter, and H. Schmidt, *Computational Ocean Acoustics* (American Institute of Physics, New York, 1994).
[21] C. W. Spofford, A synopsis of the AESD workshop on acoustic propagation modeling by non-ray-tracing techniques, 22–25 May 1973, Washington, DC, AESD TN-73-05.
[22] M. Shinozuka and C.-M. Jan, ''Digital simulation of random processes and its applications,'' J. Sound Vib. **25**, 111–128 (1972).